Journal of Power Sources 252 (2014) 333–343

Contents lists available at ScienceDirect

Journal of Power Sources

journal homepage: www.elsevier.com/locate/jpowsour

Power management optimization of fuel cell/battery hybrid vehicles with experimental validation

Farouk Odeim*, Jürgen Roes, Lars Wülbeck, Angelika Heinzel

Lehrstuhl Energietechnik, Universität Duisburg-Essen, Lotharstraße 1, 47057 Duisburg, Germany

HIGHLIGHTS

- Power management optimization of fuel cell hybrid vehicles is studied.
- New formulation for the optimization of real-time controllers is proposed.
- Real-time controllers can be optimized over many driving cycles at once.
- Three-parameter PI controller surpasses a ten-parameter fuzzy controller.

ARTICLE INFO

Article history:
Received 23 July 2013
Received in revised form
10 November 2013
Accepted 3 December 2013
Available online 13 December 2013

Keywords:
Fuel cell hybrid vehicle
Power management strategy
Optimization
Pontryagin's minimum principle
Fuzzy control
Experimental validation

ABSTRACT

Fuel cell hybrid vehicles offer a high-efficiency and low-emission substitute for their internal combustion engine counterparts. The hybridization significantly improves the fuel economy of the vehicle; however, exploiting the hybridization requires a well-designed power management strategy that optimally shares the power demand between the power sources. This paper deals with the optimization of power management strategy of a fuel cell/battery hybrid vehicle, both off-line and in real-time. A new formulation of the optimization problem for the real-time strategy is presented. The new approach allows the optimization of the controller over a set of driving cycles at once, which improves the robustness of the designed strategy. The real-time optimization is applied to two forms of real-time controllers: a PI controller based on Pontryagin's Minimum Principle with three parameters and a fuzzy controller with ten parameters. The results show that the PI controller can outperform the fuzzy controller, even though it has fewer parameters. The real-time controllers are designed by simulation and then validated by experiment.

1. Introduction

Fuel cell/battery hybrid vehicles are characterized by the use of two power sources: a fuel cell system (FCS) as the main power source and a battery as an auxiliary one. The addition of the battery leads to a significant improvement in fuel economy by restricting the operation of the FCS to high-efficiency operating points and by adding the possibility of regenerative braking. Additionally, the cruising power demand is assigned to the FCS whereas the battery helps to meet the peak power demands and, therefore, the FCS can be downsized.

The power management strategy defines the contribution of the two power sources in fulfilling a given power demand. For hybrid electric vehicles (HEVs), the main objective of any power management strategy is to minimize the fuel consumption, while limiting the variation of the state-of-charge (SOC) of the battery. Most literature has dealt with the power management of the conventional hybrid vehicles (powered by an internal combustion engine (ICE) as a main power source); however, the design and optimization approaches can be mostly adapted to the fuel cell hybrid vehicles (FCHVs). In comparison to conventional HEVs, the optimization problem is further simplified for FCHVs, since, firstly, an on/off operation of FCS is not likely (which is a normal operation of ICE and it can be optimal even during highway cruising [1]) and, secondly, FCHVs are usually equipped with a single-speed transmission and, therefore, the need for gear-ratio optimization is eliminated.

The optimal power management strategy can be obtained when the driving cycle is completely known to get the so-called off-line optimum. Dynamic Programming (DP) [2] is still the most common off-line optimization algorithm for HEVs, for it guarantees the global optimum without any assumptions regarding the convexity and

* Corresponding author. Tel.: +49 203 379 1256; fax: +49 203 379 2720.
E-mail address: farouk.odeim@stud.uni-due.de (F. Odeim).

0378-7753/$ – see front matter © 2014 Elsevier B.V. All rights reserved.
http://dx.doi.org/10.1016/j.jpowsour.2013.12.012

linearity of the system models; however, DP has the drawback that it requires a long computation time. Convex optimization has been recently applied to HEVs optimization as a significantly faster alternative to DP if the system can be described by a set of convex models and, therefore, the accuracy of the optimal solution (in comparison to DP) depends on the accuracy of the approximations done to relax the non-convex behavior of the system, if any [3,4]. Pontryagin's Minimum Principle (PMP) [2] has been successfully applied to the power management optimization of HEVs [5], where, in comparison to DP, it is very fast; however, PMP gives only the necessary conditions that must be satisfied by the global optimum and not the sufficient conditions and, therefore, the PMP solution may be a local optimum. However, if the solution of PMP is unique, then it must be a global optimum. The uniqueness of PMP solution is guaranteed if the battery model parameters are constant independent of its SOC [5].

The drawback of the off-line optimal power management strategy is that it is highly dependent on the driving cycle and, therefore, the optimal strategy over one driving cycle may result in a poor performance over other ones in real-time. Hence, designing a near-optimal real-time power management strategy is still an open issue and a matter of research. Equivalent Consumption Minimization Strategy (ECMS) has been introduced as a near-optimal real-time strategy [6–8]; however, the excellent performance of ECMS requires cycle-dependent parameters to be pre-programmed and, in Ref. [9], it has been shown that ECMS can be regarded as a realization of PMP. Since the problem associated with the off-line optimization techniques is their cycle-sensitivity, online strategy adaptation methods have been devised, where, for instance, the adaptation was based on driving pattern recognition in Ref. [10] and on driving cycle prediction in Refs. [11,12]. Stochastic Dynamic Programming has been also proposed to alleviate the cycle-sensitivity of the optimal control law [13]. Another approach to the design of real-time strategy is the static optimization, where a certain form of the real-time controller is predefined and optimized either analytically or numerically. As examples, the real-time controller took the form of an affine function of the power demand in Ref. [14], the form of Boolean rules in Ref. [15] and the fuzzy form in Refs. [16,17]. When the real-time controller is optimized over one driving cycle, then its robustness over other driving cycles becomes questionable [16,17]. In contrast, when many driving cycles of different nature are engaged in the optimization, the robustness over a random driving cycle would be more guaranteed.

This paper illustrates the idea that the real-time controllers can be optimized over a set of driving cycles at once. A comparison is made between two forms of real-time controllers: a PI controller based on PMP and a fuzzy controller. The simulation results are validated on a small-scale test stand.

The paper is structured as follows. The vehicle model is introduced in Section 2. This model is used to calculate the power demand of the evaluation driving cycles. In Section 3, the power demand is scaled down to fit the test stand and the model of the hybrid power source (fuel cell and battery) is presented. The off-line optimization using PMP is recalled in Section 4. The optimization problem of the real-time power management strategy is formulated in Section 5 and applied to two types of controllers: a PMP-based PI controller and a fuzzy controller. Experimental validation of the simulation work is illustrated in Section 6. The paper is concluded in Section 7.

2. Vehicle model

A schematic of the fuel cell/battery hybrid vehicle is shown in Fig. 1. The battery is directly connected to the bus whereas the fuel cell system is connected via a DC/DC converter. The bus feeds the motor which, in its turn, drives the vehicle wheels.

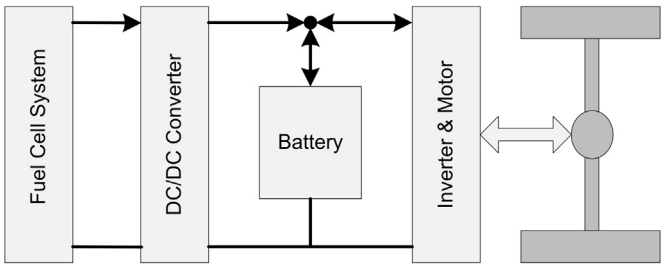

Fig. 1. Schematic of fuel cell hybrid vehicle.

The vehicle model aims to calculate the electric power required by the hybrid power source to meet a given speed profile, $v(t)$. The traction force, F_t, required at the wheels for a given speed is the sum of four forces:

$$F_t = F_{acc} + F_a + F_r + F_g \tag{1}$$

where F_{acc} is the force required to accelerate the vehicle, F_a is the force required to overcome the aerodynamic drag, F_r is the one to overcome the rolling friction with the road surface and F_g is the gravity force acting on the vehicle when driving on non-horizontal roads (up or downhill). These forces are given in (2).

$$\begin{aligned} F_{acc} &= \left(m + \frac{\Theta_w}{r^2}\right)\frac{dv}{dt} \\ F_a &= \tfrac{1}{2}\rho\, C_d A_f v^2 \\ F_r &= \begin{cases} mg(\mu_0 + \mu_1 v)\cos(\alpha) & v > 0 \\ 0 & v = 0 \end{cases} \\ F_g &= mg\sin(\alpha) \end{aligned} \tag{2}$$

The parameters of the vehicle model are listed in Table 1.The road angle, α, is assumed 0 for all the evaluation driving cycles. Given the traction force, the required torque at the wheel, $T_w = rF_t$, and the wheel rotational speed, $w_w = v/r$, are then obtained. The transmission line is modeled by its efficiency, η_{tr}, and gear ratio, R. The motor torque, T_{m1}, and its rotational speed, w_m, is then given by

$$\begin{aligned} T_{m1} &= \begin{cases} T_w/(R\eta_{tr}) & T_w \geq 0 \\ T_w\eta_{tr}/R & T_w < 0 \end{cases} \\ w_m &= Rw_w \end{aligned} \tag{3}$$

In the dynamic state, the actual mechanical torque, T_m, produced by the motor is given by

$$T_m = T_{m1} + \Theta_m \frac{dw_m}{dt} \tag{4}$$

Given T_m and w_m, the input electric power can be calculated using the efficiency map of the motor and its driver, η_m, as expressed in (5). The efficiency map is shown in Fig. 2.

Table 1
Parameters of the vehicle model.

Parameter	Value
Vehicle mass, m (kg)	1500
Wheels inertia, Θ_w (kg m^2)	4
Motor inertia, Θ_m (kg m^2)	0.1
Wheel radius, r (m)	0.305
Gravity constant, g (m s^{-2})	9.8
Friction coefficients; μ_0, μ_1 (m^{-1} s)	0.007, 0.00012
Aerodynamic drag coefficient, C_d	0.3
Air density, ρ (kg m^{-3})	1.2
Vehicle frontal area, A_f (m^2)	1.75
Gear ratio, R	8.9
Transmission efficiency, η_{tr}	0.95

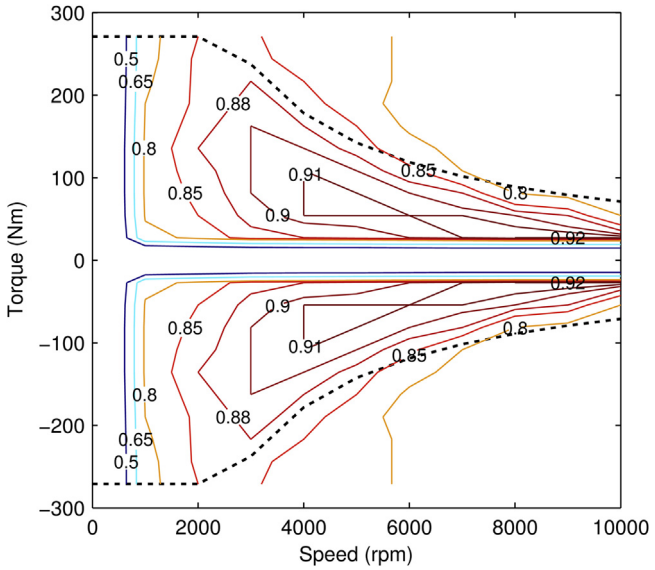

Fig. 2. Efficiency map of the motor and its driver. The dotted line represents the torque limits. Data taken from the ADVISOR model of a Westinghouse 75-kW AC induction motor.

$$P_{\text{dem}} = \begin{cases} T_{\text{m}} w_{\text{m}} / \eta_{\text{m}} & T_{\text{m}} > 0 \\ \eta_{\text{m}} T_{\text{m}} w_{\text{m}} & T_{\text{m}} < 0 \\ 0 & T_{\text{m}} = 0 \end{cases} \quad (5)$$

3. Hybrid power source

The optimization results will be validated on a test stand composed of a fuel cell system, DC/DC converter, 10-cell lithium-polymer battery and two-quadrant load. The battery cells have lithium nickel manganese cobalt oxide ($LiNiMnCoO_2$) as a cathode material and graphite as an anode material.

The test stand is supposed to simulate the vehicle on a small scale. The hybrid power source of the vehicle has a maximum fuel cell power of 50 kW, maximum/minimum battery power of ±30 kW, nominal bus voltage of 320 V and battery capacity of 7 Ah. The test stand is equipped with a 1.2 kW fuel cell system, which is used to calculate the scaling factor of 0.024 (=1.2 kW/50 kW). The battery power limits, battery energy and the power profiles calculated from the vehicle model are scaled down by the same factor. So, the battery power is limited in the test stand to ±0.72 kW (= ±30 kW × 0.024). The vehicle battery has an energy of 2240 Wh (=7 Ah × 320 V) and, therefore, the battery of the test stand should have an energy of 54 Wh (=2240 Wh × 0.024). Assuming a 37 V nominal battery voltage in the test stand, a 1.5 Ah battery capacity is required in the test stand.

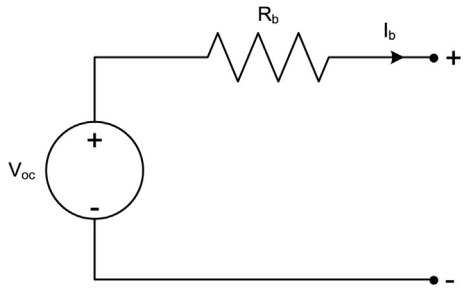

Fig. 3. Internal-resistance model of the battery.

Actually, the battery used has a capacity of 30 Ah, which is quite large in comparison to the required capacity. So, only 1.5 Ah from the entire capacity is considered around 60% SOC, and the reported experimental SOC corresponds to the required capacity and not to the actual one. This has an implication on the battery model. Although many battery models have been developed [18], the internal-resistance model (Fig. 3) is still the most often used model for HEV supervisory control, due to its simplicity for a quick simulation. In this model, the battery is represented by its open circuit voltage, V_{oc}, in series with its internal resistance, R_{b}. Two values of R_{b} are usually distinguished: one when charging the battery and the other when discharging it. All the model parameters vary with the SOC as shown in Fig. 4. The parameters were identified by an HPPC test (Hybrid Pulse Power Characterization Profile) [19]. Since only small part of the capacity will be used, a constant open circuit voltage of 37.37 V and a constant internal resistance of 37 mΩ are used in the simulation. These values correspond to 60% SOC. It should be noted that the use of constant battery model parameters has no significant effects on the transferability of our experimental results to the real world applications, since, on the vehicle level, the battery is operated over a narrow SOC range (∼45%–75%) and, over such range, the open circuit voltage and the internal resistance of the battery do not vary significantly with SOC, as illustrated in Fig. 4.

The hydrogen consumption rate, $\dot{m}_{\text{h}}$, was measured as a function of the output power of the DC/DC converter, P_{dc}, and the relation is modeled by a quadratic polynomial (Fig. 5) over the range 0–750 W, which is a sufficient range for all the evaluation driving cycles that will be used. In comparison to the linear interpolation between the measurement data, using a differentiable model results in a smoother control of the system. The combined efficiency of the FCS and DC/DC converter is defined as the ratio of P_{dc} to the hydrogen power, $\dot{m}_{\text{h}} \times \text{LHV}$, where LHV (=120 kJ g^{-1}) is the lower heating value of hydrogen. A comparison between the measured efficiency and the model efficiency is illustrated in Fig. 6.

4. Off-line optimization

The off-line optimal power management strategy stands for the strategy that moves the system from an initial state x_0 at the beginning of the driving cycle ($t = 0$) to a final state x_{f} at the end of

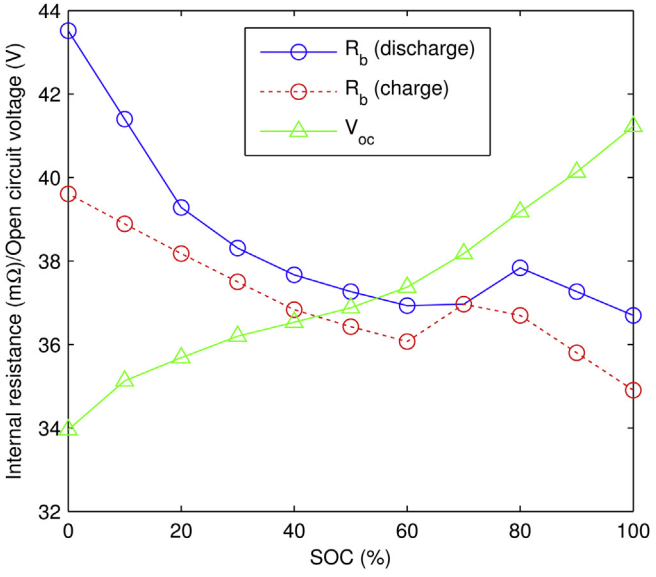

Fig. 4. Parameters of the battery internal-resistance model as a function of SOC.

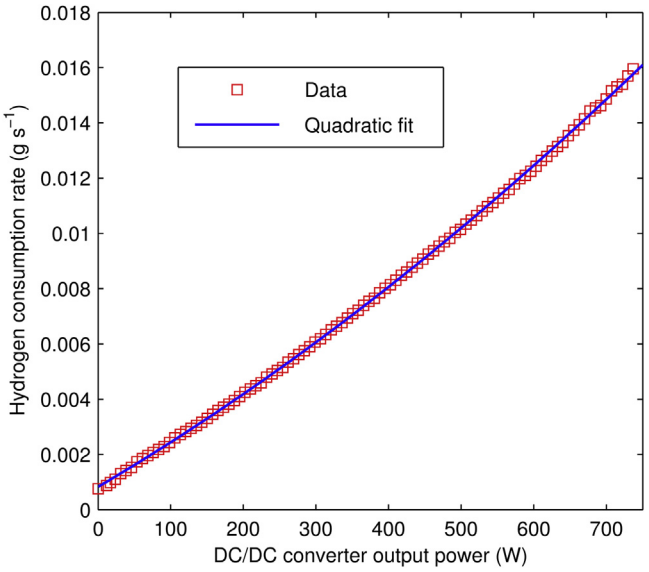

Fig. 5. Experimental hydrogen consumption rate versus output power of DC/DC converter with a quadratic polynomial fit to the data.

the driving cycle ($t = t_f$) while minimizing the hydrogen consumed over the driving cycle. Pontryagin's Minimum Principle (PMP) is used to find the optimal solution [2,5,9,12].

The power demand, P_{dem}, is the sum of battery power, P_b, and the power of the DC/DC converter, P_{dc}.

$$P_{dem} = P_{dc} + P_b \tag{6}$$

The state-of-charge of the battery is used as the only state of the system (i.e., $x \equiv$SOC), which is calculated according to (7) and governed by the dynamic Equation (8),

$$x(t) = x_0 - \frac{1}{Q_b}\int_0^t I_b(\tau)\mathrm{d}\tau \tag{7}$$

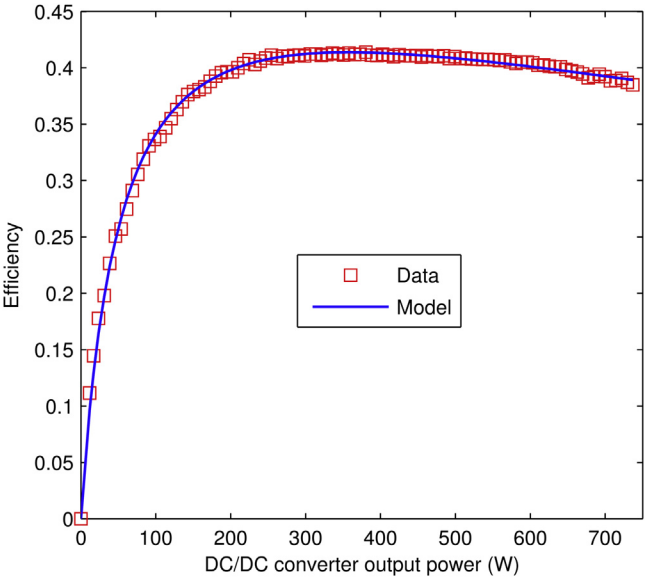

Fig. 6. Combined efficiency of fuel cell system and DC/DC converter.

$$\dot{x}(t) = \frac{-I_b}{Q_b} = -\frac{1}{2R_bQ_b}\left(V_{oc} - \sqrt{V_{oc}^2 - 4R_bu(t)}\right) = f(x(t), u(t)) \tag{8}$$

where u is the battery power, which is used as a control variable. I_b and Q_b are the battery current and battery capacity, respectively. The battery power and current are considered positive for discharging and negative for charging.

The power of DC/DC converter is bounded between a minimum, $P_{dc,min}$, and a maximum, $P_{dc,max}$. Likewise, the battery power is bounded between $P_{b,min}$ and $P_{b,max}$. These power constraints impose a limitation on the control variable, u, as follows:

$$u \in \mathbf{U}(t) \equiv \lfloor \max(P_{dem}(t) - P_{dc,max}, P_{b,min}), \min(P_{dem}(t) - P_{dc,min}, P_{b,max}) \rfloor \tag{9}$$

The cost function to be minimized is the total hydrogen consumption, M, and it is given by:

$$M = \int_0^{t_f} \dot{m}_h(u(t), t)\mathrm{d}t \tag{10}$$

The Hamiltonian of the system is defined as:

$$H(x(t), u(t), \lambda(t), t) = \dot{m}_f(u(t), t) - \lambda(t) f(x(t), u(t)) \tag{11}$$

where $\lambda(t)$ is called the co-state, which is, in general, a function of time. The Minimum Principle states that the optimal control variable minimizes the Hamiltonian, that is:

$$H\left(x^0(t), u^0(t), \lambda^0(t), t\right) \le H\left(x^0(t), u, \lambda^0(t), t\right) \quad \forall t \in \left[0, t_f\right], \forall u \in \mathbf{U}(t) \tag{12}$$

where $x^0(t)$ is the optimal state trajectory which results from the optimal control $u^0(t)$ and the initial state x_0, and $\lambda^0(t)$ is the optimal co-state trajectory, whose dynamics is governed by

$$\dot{\lambda}^0(t) = \frac{\partial H}{\partial x}\left(x^0(t), u^0(t), \lambda^0(t), t\right) = -\lambda^0(t)\frac{\partial f}{\partial x}\left(x^0(t), u^0(t)\right) \tag{13}$$

The function f in (8) is, in general, a function of x, since the V_{oc} and the R_b vary with x; however, as stated in Section 3, these two parameters are assumed constant and, therefore, f is independent of x in our case. As a result, according to (13), the optimal co-state is constant. In this special case, where the optimal co-state is constant, the solution of PMP, if exists, is unique and it is a global optimum [5].

For a given co-state, the Hamiltonian is minimized at each time step over the permissible control range to find the optimal control. The co-state plays the role of a weighting factor, so that for a high co-state the charging of the battery is favored and the final SOC tends to be high, and for a low co-state, the final SOC tends to be low. As a result, the optimal co-state depends on the final SOC, x_f, which is a predefined parameter of the optimization problem. So, finding the optimal co-state which leads to a certain x_f requires an iterative procedure over the entire driving cycle. The iteration stops once the required x_f is obtained. Making use of the last remark, that x_f is a monotonically increasing function of λ, a binary search algorithm can be used to find the optimal co-state within few iterations. The search algorithm uses an initial search space $[\lambda_{min}, \lambda_{max}]$. Theoretically, λ is limited between zero and infinity, where a zero co-state minimizes the Hamiltonian at the minimum

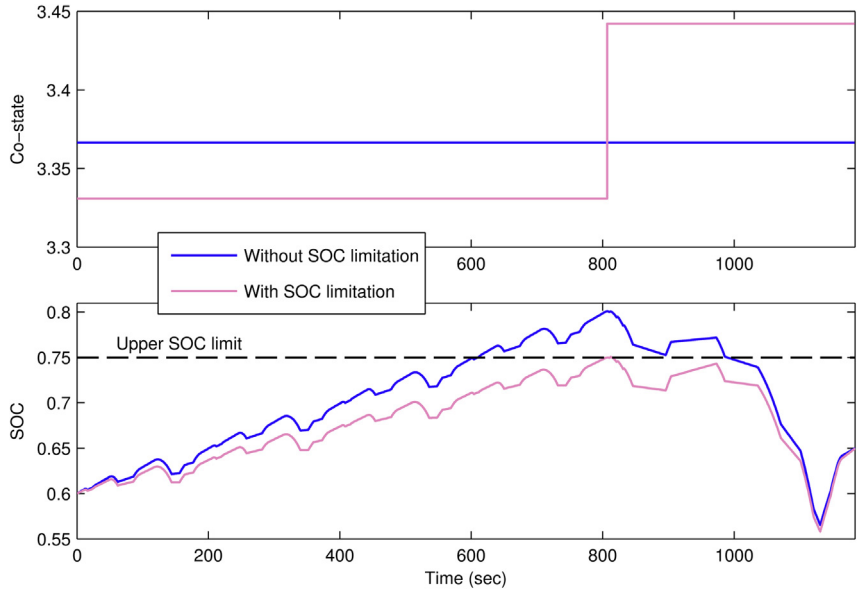

Fig. 7. Optimal PMP co-state (top) and state (bottom) trajectories over NEDC with and without SOC limitation.

possible P_{dc} (maximum possible P_b) and an infinite co-state results in the maximum possible P_{dc} (minimum possible P_b). In the search algorithm, the initial λ_{min} is set to zero whereas the initial λ_{max} is set to 4 which is more than enough for our system. The algorithm starts by testing λ_{av}, the average of λ_{min} and λ_{max}. If the achieved final SOC is lower than the required one, λ_{min} is increased to λ_{av}, and if the achieved SOC is higher than the required one, λ_{max} is decreased to λ_{av}. In the next iteration, the procedure is repeated with the new search limits. At the end of each iteration, the size of the search space is halved and, within 10 iterations, the space size is reduced to less than 0.1% of its initial value.

The SOC of the battery is to be limited between $x_{min} = 0.45$ and $x_{max} = 0.75$ at any time of the driving cycle. The PMP, as stated, does not include the SOC limitation, in contrast to other optimization algorithms like Dynamic Programming. There are several approaches that can be used to incorporate the state constraint into the formulation of PMP [2,20]. The approach used here was introduced in Ref. [21] and can be summarized as follows: the optimal state trajectory is calculated first for the entire driving cycle. If the solution satisfies the state constraints, then the obtained solution is the optimum. Otherwise, the load profile is divided into two sub-profiles at the time step where the maximum violation of state limits occurs, and the optimization is repeated for each sub-profile. If the upper state limit is violated, then x_{max} is used as a final state for the first sub-profile and as an initial state for the second one. Otherwise, if the lower state limit is violated, then x_{min} is used as a final state for the first sub-profile and as an initial state for the second one. The division is repeated within each sub-profile if the state constraint is violated again, until the state constraints are satisfied for all sub-profiles. Fig. 7 illustrates the algorithm used to consider the SOC limitation in PMP. Here the objective is to find the optimal PMP solution over NEDC driving cycle for an initial SOC, x_0, of 0.6 and a final SOC, x_f, of 0.65. At first, the optimal state and co-state trajectories are calculated over the entire driving cycle between $t = 0$ and $t_f = 1184$ s without SOC limitation. In this case, a violation of the upper SOC limit is observed and the maximum violation occurs at the time step $t_c = 807$ s. As a result, the power demand profile of NEDC is divided into two sub-profiles, $P_{dem1} = P_{dem}$ ($[0,t_c[$) and $P_{dem2} = P_{dem}$ ($[t_c,t_f]$). Over the time span $[0,t_c]$, the optimization problem is re-solved with an initial state x_0 and a final state $x_{max} = 0.75$, whereas, over the time span $[t_c,t_f]$, the optimization problem is re-solved for an initial state x_{max} and a final state x_f. In this case, no further sub-division is required since the two optimal SOC sub-trajectories do not violate the limitations. The calculated two co-state sub-trajectories and the two state sub-trajectories are simply combined at t_c to form the PMP solution with SOC limitation. Comparing the unconstrained and constrained co-state trajectories in Fig. 7, an interesting feature of the co-state is observed when the SOC limits are hit. The optimal co-state over the time span $[0,t_c[$ is lower than that of the unconstrained solution since the achieved final state is lower, and the optimal co-state over the time span $[t_c,t_f]$ is higher than that of the unconstrained solution since the initial state is lower. This explains the jump in co-state at t_c.

To sum up, the objective and constraints of the off-line optimization are summarized as follows:

$$\begin{aligned} &\text{Objective :} && \min \int_0^{t_f} \dot{m}_h(u(t),t)\mathrm{d}t \\ &\text{Constraints :} && \dot{x}(t) = f(u(t)) \\ & && x_0 = x(0) \\ & && x_f = x(t_f) \\ & && x_{min} \le x \le x_{max} \\ & && P_{b,min} \le P_b \le P_{b,max} \\ & && P_{dc,min} \le P_{dc} \le P_{dc,max} \end{aligned} \tag{14}$$

5. Real-time optimization

In case of off-line power management strategies, the driving cycle is assumed to be known in advance and an end SOC constraint is assumed. For perfect charge sustenance, the final SOC is required to be the same as the initial one (i.e., $x_f = x_0$). In contrast, for real-time strategies, the future driving pattern is not known and, therefore, the end SOC will not necessarily be the same as the initial one.

When designing a real-time power management strategy, this strategy should be compared with other strategies, including the optimal one, to evaluate it. Since different strategies may result in different end SOC, the comparison based only on the fuel

consumption is not a reasonable approach. So, an algorithm is required to quantitatively compare the real-time strategies.

The algorithm used here, is to refer the fuel consumption of any strategy to the same reference final SOC, $x_{f,ref}$. The final SOC of 0.6 is used as a reference one. In this case, we need to define the equivalent fuel consumption.

5.1. Equivalent fuel consumption

The equivalent fuel consumption is defined as the fuel consumption of the strategy under interest if the final state of charge were the reference one. The definition of the equivalent fuel consumption is illustrated in Fig. 8. The off-line optimization problem is solved for various final SOC, x_f, and the resulting fuel consumption, $M_{opt} = f(x_f)$, is shown in Fig. 8 for the driving cycle NEDC, as an example. The resulting off-line optimal curve is then used to correct the difference between x_f and $x_{f,ref}$ [22]. If, for a real-time power management strategy, a final SOC of x_f and a fuel consumption of M are achieved (as represented by the circle), a curve parallel to the optimal consumption curve is constructed starting from x_f and ending at $x_{f,ref}$ (the end is represented by a triangle). Then the equivalent fuel consumption, M_{eq}, is the y-coordinate at the end of the curve. This is expressed in (15), where $M_{opt,ref}$ is the optimal hydrogen consumption for $x_f = x_{f,ref}$.

$$M_{eq} = M - M_{opt}\left(x_f\right) + M_{opt,ref} \tag{15}$$

5.2. Optimization problem formulation

Any real-time power management strategy has parameters that can be optimized for a given driving cycle in terms of hydrogen consumption and charge sustenance. However, the optimized parameters for a driving cycle may behave poorly for another, so it would be better to incorporate many driving cycles in the optimization problem. In this case, the probability of a poor performance over a random driving cycle decreases. The objective of the real-time power management strategy is to achieve fuel consumption as close as possible to the off-line optimal one while keeping the SOC in an acceptable range.

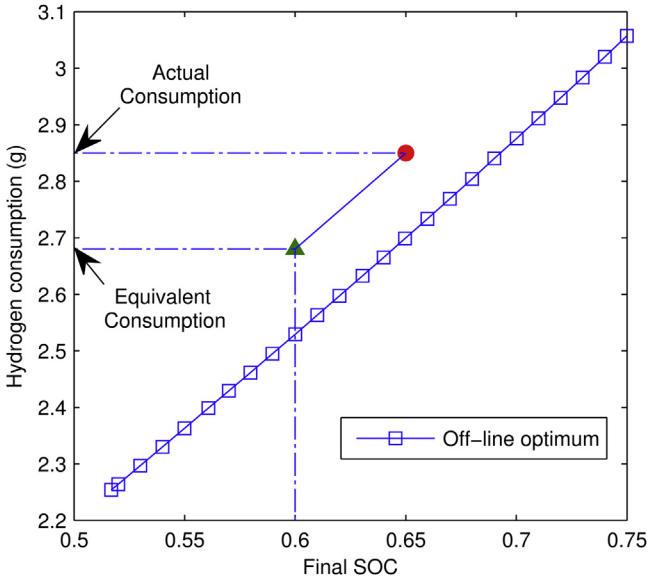

Fig. 8. Off-line optimal hydrogen consumption over NEDC versus final SOC for an initial SOC of 0.6, and an example calculation of the equivalent fuel consumption.

The approach used here accounts for fuel consumption and charge sustenance as two separate performance indices. For a given driving cycle, i, we define two performance indices of the real-time strategy: one for hydrogen consumption, J^i_{HC}, and the other for charge sustenance, J^i_{SOC}, as follows:

$$\begin{aligned} J^i_{HC} &= \frac{M^i_{eq} - M^i_{opt,ref}}{M^i_{opt,ref}} \times 100(\%) \\ J^i_{SOC} &= \left| x^i_f - x_{f,ref} \right| \end{aligned} \tag{16}$$

The first performance index measures how far the hydrogen consumption of the real-time strategy is from the off-line optimal consumption, whereas the second one measures the deviation from the perfect charge sustaining performance. It is important to notice that the definition of the performance indices does not distinguish between positive or negative $(x^i_f - x_{f,ref})$ if the equivalent consumption is the same.

For a set of driving cycles, we define the total performance indices as follows:

$$\begin{aligned} J_{HC} &= \frac{1}{N}\sum_i J^i_{HC} \\ J_{SOC} &= \max_i J^i_{SOC} \end{aligned} \tag{17}$$

where J_{HC} is the total performance index for hydrogen consumption, i.e., the average of individual indices of all driving cycles, where N is the number of driving cycles incorporated in the optimization. Each set of the controller parameters results in a value for the two performance indices and the objective of the optimization is to find the parameters which minimize the fuel consumption while the final SOC of all driving cycles lie within a predefined range. The optimization problem can be formulated as follows:

$$\begin{aligned} &\text{Objective :} && \min J_{HC} \\ &\text{Constraints :} && x_{min} \le x^i(t) \le x_{max} \quad \forall t \in \left[0, t^i_f\right] \quad \forall i \\ & && J_{SOC} \le \alpha \end{aligned} \tag{18}$$

The first constraint states that the SOC trajectory of all driving cycles must stay within the allowed limits. The second constraint defines the maximum SOC deviation from the reference at the end of driving cycles. The optimization problem can be solved for varying α. With increasing α, the window of parameters, over which J_{HC} is minimized, expands and, therefore, a smaller objective value is obtained.

5.3. Real-time controllers

Two real-time controllers are to be optimized. The first controller is based on PMP and has a PI form with three parameters, and the second one is a fuzzy controller with ten parameters.

The form of the PI controller is given in (19). It controls the SOC around the reference, $x_{ref} = 0.6$, and outputs the co-state which is then used in real-time when minimizing the Hamiltonian defined in (11). This type of controller was used in Refs. [23,24], as examples. The controller has three parameters that can be optimized: the initial co-state, λ_0; the proportional gain, K_p; and the integral gain, K_i.

$$\lambda(t) = \lambda_0 + K_p\left(x_{ref} - x(t)\right) + K_i \int_0^t \left(x_{ref} - x(\tau)\right) d\tau \tag{19}$$

The fuzzy controller has two inputs (power demand and battery SOC) and one output (power of DC/DC converter). Trapezoidal

membership functions are used for the inputs and the output, with 4 parameters defining the membership functions of each variable: SOC ($x_1 \ldots x_4$), P_{dem} ($y_1 \ldots y_4$) and P_{dc} ($z_1 \ldots z_4$), respectively, as shown in Fig. 9. This controller has a relatively low resolution with three membership functions for each variable, which are denoted as L (Low), M (Medium) and H (High). The rules of the controller are listed in Table 2. The logic behind these rules is as follows: P_{dc} is set to high if the SOC is low regardless of P_{dem} level (low, medium or high) in order to charge the battery. If the SOC is around the reference (i.e., SOC is medium), P_{dc} follows the level of P_{dem} in an attempt to keep the SOC in the medium range. If the SOC is high, P_{dc} is set to a level lower than that of P_{dem} when P_{dem} is medium or high in order to discharge the battery. The membership functions of SOC are assumed to be symmetrical around the reference 0.6; i.e., knowing x_1 and x_2 gives x_3 and x_4. So, the parameters engaged in the optimization counts 10: $x_1 - x_2, y_1 - y_4, z_1 - z_4$. The parameters of a fuzzy controller may be defined by various means. In Ref. [17], for example, the fuzzy controller has the same resolution (i.e., three membership functions for each variable) and is defined by only five parameters, whereas a higher resolution is used in Ref. [16] with 22 parameters. Generally speaking, increasing the number of parameters increases the dimension of the optimization problem and, therefore, a better controller performance is expected; however, this comes at the expense of increased optimization time.

In contrast to the PI controller, the optimal fuzzy logic controller (with respect to the optimization problem defined in (18)) does not necessarily respect the system power constraints (9). So, it is possible for a set of controller parameters that certain power demands are not met by the controller even though the power source is physically capable of fulfilling them. As a workaround, a dynamic saturation element is added at the output of the controller to hardly force the output to be within the limits allowed by the system. The lower, $P_{dc,lo}$, and upper, $P_{dc,up}$, bounds of the saturation element varies with power demand as follows:

$$\begin{aligned} P_{dc,lo}(t) &= \max(P_{dem}(t) - P_{b,max}, P_{dc,min}) \\ P_{dc,up}(t) &= \min(P_{dem}(t) - P_{b,min}, P_{dc,max}) \end{aligned} \quad (20)$$

Genetic algorithm [25] was used to optimize the two controllers, PI and fuzzy, with a fitness function and constraints as defined in (18) with $\alpha = 0.05$ (i.e., the final SOC of any driving cycle must be between 0.55 and 0.65). Five driving cycles are engaged in the optimization, namely, NEDC, UDDS, NYCC, Japanese 10–15 and HWFET, whereas US06 is used later to test the robustness of the controllers. The genetic algorithm was run for 100 generations and the population size was chosen to be 10 times the number of controller parameters, i.e., 30 for PI and 100 for fuzzy. The optimization procedure proceeds as follows: For each set of parameters (i.e., individual) generated by the genetic algorithm, the corresponding controller is tested over each driving cycle separately, where all driving cycles are initiated with an SOC of 0.6. If the controller satisfies the constraints of the problem (18), the corresponding objective function, J_{HC}, is calculated according to Equations (16), (17). Otherwise, a high value is assigned to the corresponding objective function in order to cause the algorithm to go away from the selected parameters in the subsequent generation.

Table 2
Rule list of the fuzzy logic controller.

P_{dc}		SOC		
		L	M	H
P_{dem}	L	H	L	L
	M	H	M	L
	H	H	H	M

The results of the optimization show that the PI controller excels the fuzzy controller. The optimal J_{HC} of the PI controller is 0.28% whereas it is 0.74% for the fuzzy controller. Those values of J_{HC} are attained for J_{SOC} of 0.05 (i.e., the maximum allowed J_{SOC}). As defined by Equations (16), (17), the optimal J_{HC} represents the minimum average deviation from the off-line optimal fuel consumption, where the average is evaluated over the driving cycles engaged in the optimization. The optimal PI controller parameters are as follows: $\lambda_0 = 3.37$, $K_p = 3.10$ and $K_i = 4.70 \times 10^{-5}$. A surface plot of the optimal fuzzy logic controller, together with the output limitation defined in (20), is shown in Fig. 10. The message of these findings is the following: the PMP-based PI controller with only three parameters can perform, on average, better than a fuzzy logic controller with ten parameters. However, the difference between the two controllers is so small, that an experimental validation is conducted for a fairer judgment.

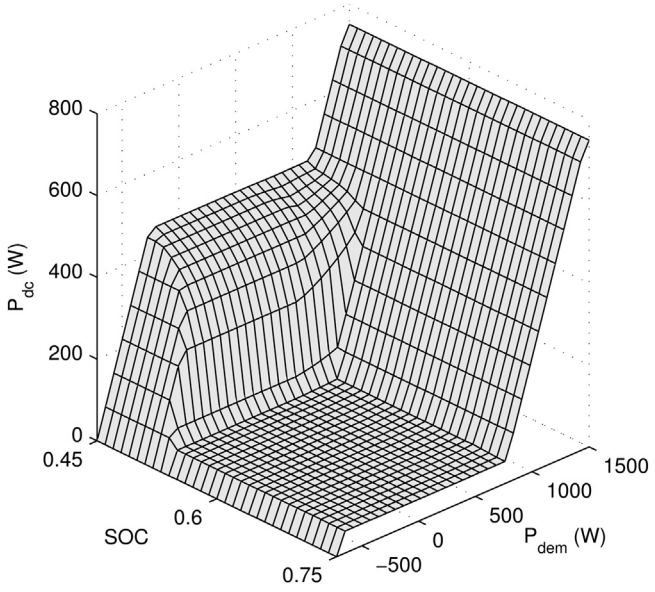

Fig. 10. Surface view of the optimized fuzzy controller with the output limitation.

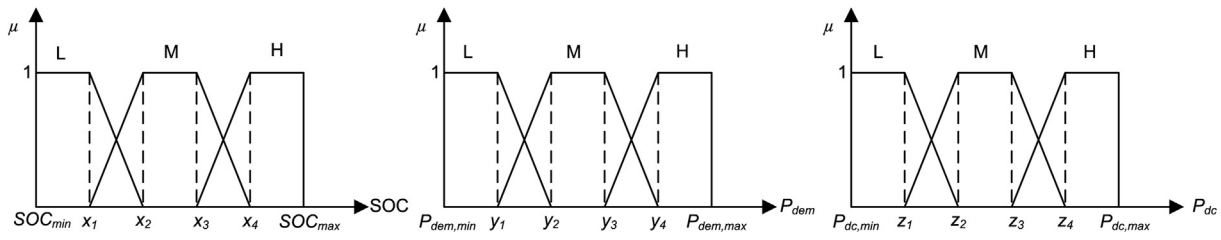

Fig. 9. Membership functions of the fuzzy controller.

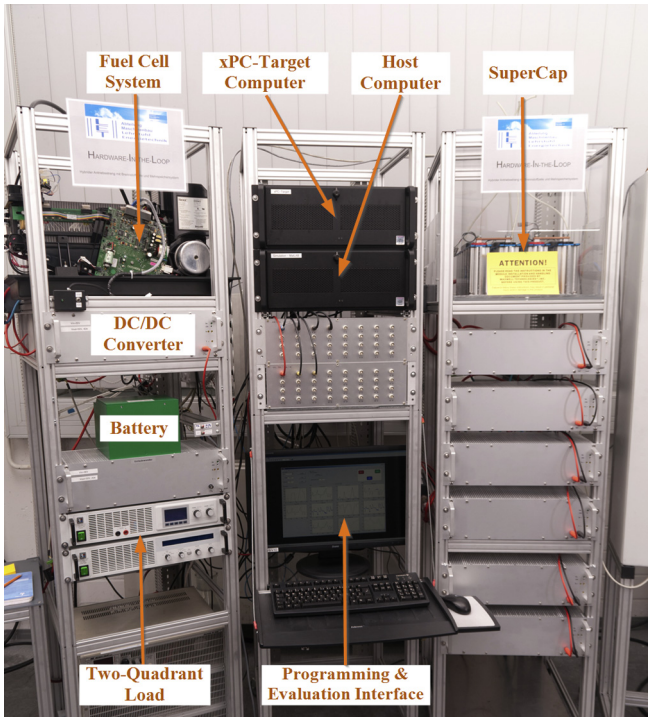

Fig. 11. Photograph of the Hardware-in-the-Loop test stand.

6. Experimental validation

The results obtained by the simulation and optimization are experimentally validated in this section, both in open loop and closed loop. The off-line optimality is validated in open loop, whereas in closed loop, the performance of the two optimized real-time controllers, PI and fuzzy, is evaluated on the test stand.

The Hardware-in-the-Loop test stand (Fig. 11) is composed of a fuel cell system, DC/DC converter, lithium-polymer battery and two-quadrant load to simulate both driving phase and regenerative braking. The output current of the DC/DC converter is controlled by the power management strategy. The whole test stand is controlled and monitored in real-time by an xPC-Target computer equipped with fast and high-resolution input/output cards. The target application is programmed in Simulink environment on a host computer. The communication between the target computer and the host computer serves to download the compiled application to the target computer and to transfer the collected data from the target to the host computer for evaluation.

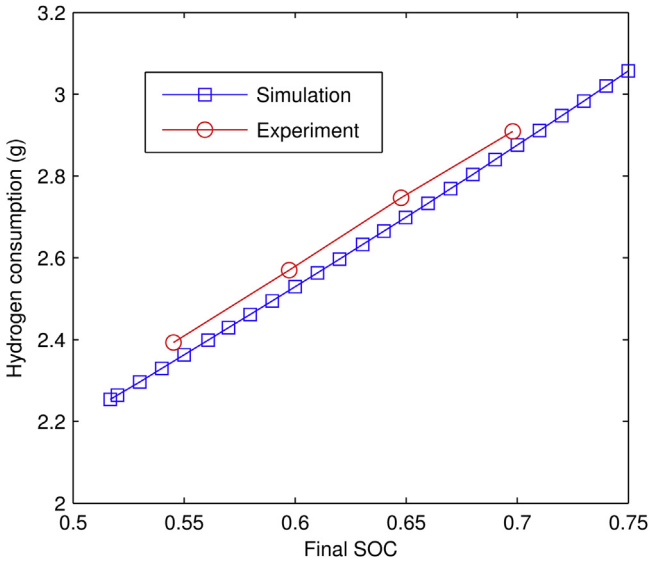

Fig. 13. Off-line optimal fuel consumption over NEDC as a function of final SOC in simulation and experiment.

6.1. Open loop validation

NEDC was used to test the behavior of the hardware in open loop. The off-line optimal co-state trajectories calculated by the off-line optimization are applied to the experimental power management strategy which includes the minimization of the Hamiltonian. Four co-state trajectories were chosen for validation corresponding

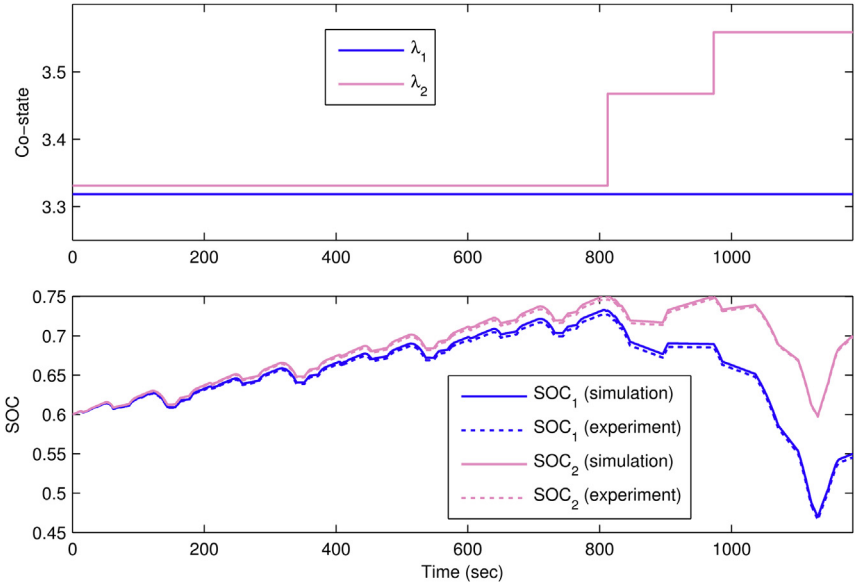

Fig. 12. Open loop behavior of the test stand. (Top) off-line optimal co-state trajectories and (bottom) the resulting state trajectories in simulation and experiment. The subscripts 1 and 2 link the co-state trajectories in the upper sub-figure with the resulting SOC trajectories in the lower one.

Table 3
Experimental results of the PI and fuzzy controllers over the evaluation driving cycles.

	NEDC		UDDS		NYCC		Japan. 10-15		HWFET		US06	
	PI	Fuzzy	PI	Fuzzy	PI	Fuzzy	PI	Fuzzy	PI	Fuzzy	PI	Fuzzy
x_f	0.558	0.568	0.638	0.548	0.649	0.646	0.626	0.579	0.551	0.569	0.608	0.546
M (g)	2.472	2.578	3.032	2.764	1.046	1.055	1.697	1.548	3.015	3.135	1.631	1.449
M_{eq} (g)	2.612	2.686	2.907	2.936	0.888	0.905	1.612	1.617	3.193	3.249	1.603	1.633

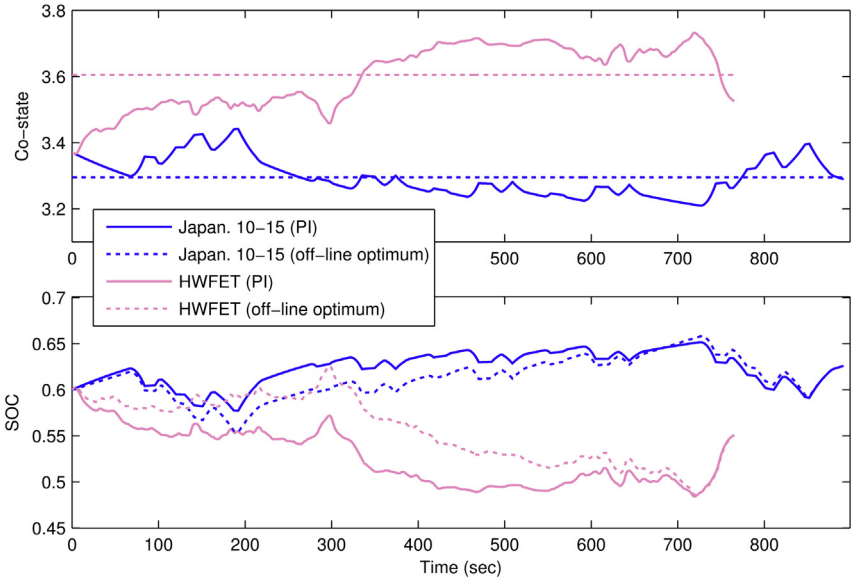

Fig. 14. Experimental co-state (top) and state (bottom) trajectories for the PI controller over Japanese 10–15 and HWFET. The simulation off-line optima are also shown.

to final SOC of 0.55, 0.6, 0.65 and 0.7. Fig. 12 shows the first and fourth co-state trajectories together with the corresponding simulation and experimental state trajectories. The other two trajectories are dropped out for the sake of clarity. As can be seen from Fig. 12, the optimal co-state makes a step-up when the state trajectory hits the upper state limit of 0.75 (as discussed in Section 4).

The small discrepancy in state trajectory between simulation and experiment results from the instrumentation error, mainly, from the error in following the load profile. Fig. 13 shows the corresponding experimental hydrogen consumption, which is slightly higher than the simulation optimum due to the error in modeling of the fuel cell system and DC/DC converter and, mainly, from the

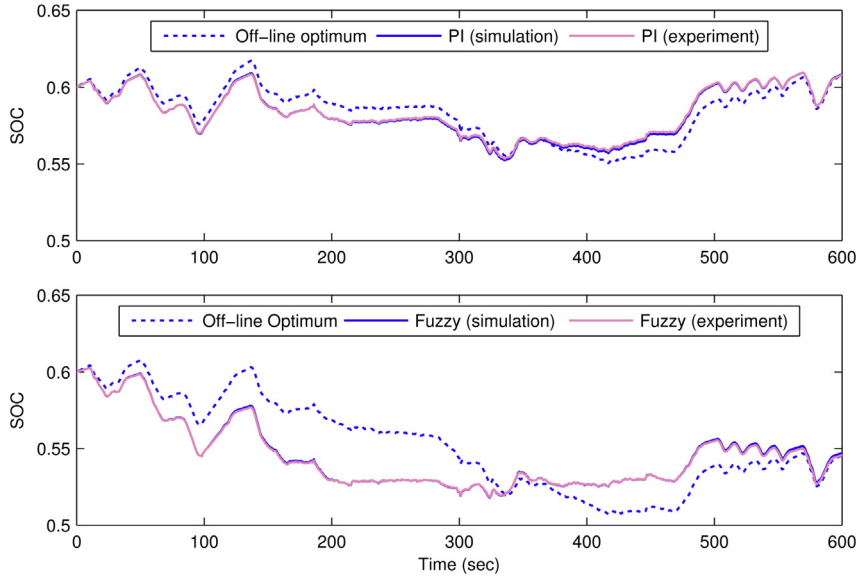

Fig. 15. State trajectories of the US06 for the PI (top) and fuzzy (bottom) controllers with the corresponding off-line optimum.

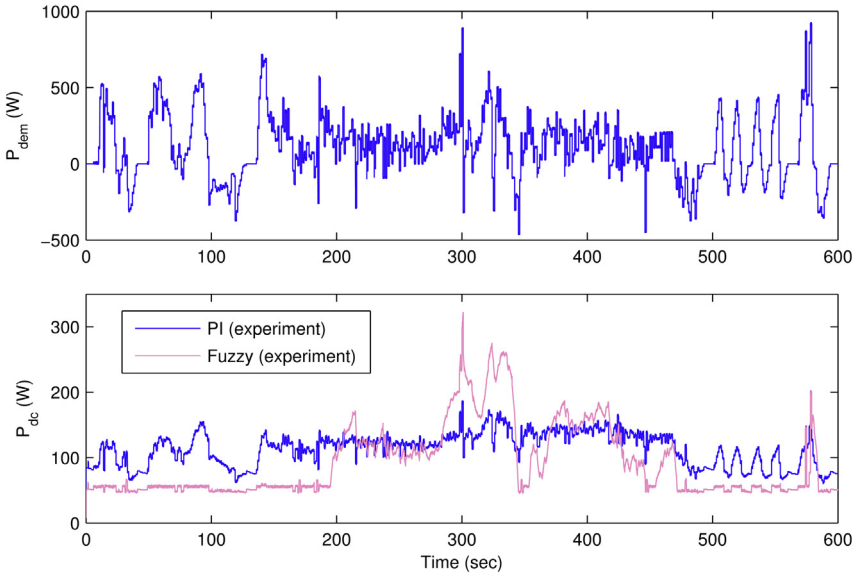

Fig. 16. (Top) US06 power profile and (bottom) the output power of the DC/DC converter for the PI and fuzzy controllers.

transient efficiency which is not taken into account in the models. As will be illustrated in the next subsection, the open loop evaluation is required if the real-time strategy is to be compared with the off-line optimum.

6.2. Closed loop validation

The two controllers, the PMP-based PI and fuzzy controllers optimized in Section 5.3, were tested on the test stand in terms of fuel consumption and achieved final SOC, and the results are listed in Table 3. The equivalent consumption, M_{eq}, is calculated as described in Section 5.1. The results show first that both controllers obey the design criterion that the SOC at the end of each driving cycle must stay within ±0.05 from the reference SOC of 0.6. The fuzzy controller deviates a bit from the criterion for UDDS. The second finding is that the PI controller excels the fuzzy controller in terms of fuel consumption. The improvement in fuel consumption ranges from 0.3% for Japanese 10–15 to 2.8% for NEDC.

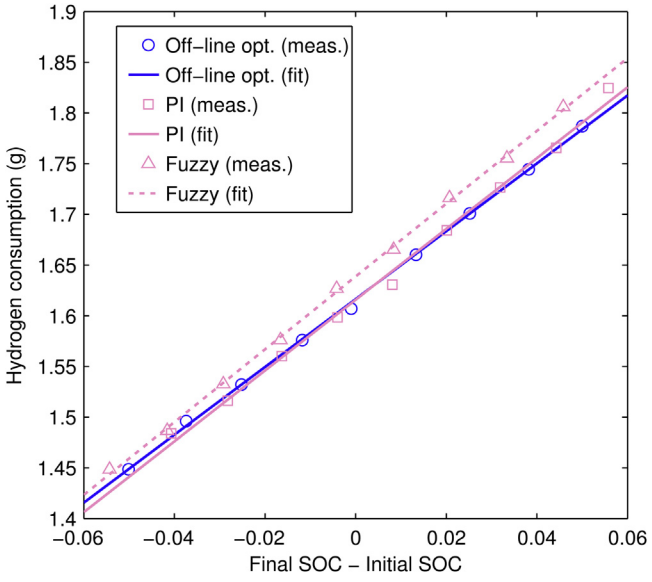

Fig. 17. Experimental hydrogen consumption for the off-line optimum, the PI controller and the fuzzy controller versus the difference between the final and initial SOC, with the corresponding linear polynomial fits. "opt." stands for "optimum" and "meas." stands for "measurement."

The idea behind the use of a PI controller for the co-state is illustrated in Fig. 14, which shows the experimental co-state and state trajectories for Japanese 10–15 and HWFET. The same controller works for these two different driving cycles, so that the SOC trajectory respects the SOC limits and the final SOC is in the range 0.55–0.65, which are the two design constraints of the controller. If no co-state adaptation is used (i.e., the proportional and integral parameters are set to zero and, therefore, the initial co-state $\lambda_0 = 3.37$ is kept constant over the entire time horizon), the simulation shows that HWFET will end up at SOC of 0.23 and Japanese 10–15 will end up at SOC of 0.75, if no SOC limitations are considered. This means that a constant co-state of 3.37 is too small for HWFET and too high for Japanese 10–15; however, online adaptation of the co-state via a feedback controller of the SOC works for different driving cycles.

The performance of the two controllers was, additionally, evaluated over US06, where US06 had not been included in the optimization of the controllers. The speed profile of US06 was scaled down to a maximum of 80 km h^{-1} to fit our vehicle model. The results for US06 are reported in the last two columns of Table 3. Also here the PI controller saves about 1.8% of hydrogen in comparison to the fuzzy controller. Fig. 15 illustrates a comparison between the off-line optimal, the simulation, and the experimental state trajectories of the US06. The simulation reproduces the experimental results very well for both controllers. The PI controller results in a state trajectory closer to the off-line optimum

Table 4
Comparison between the pure fuel cell drive and the hybrid drive in terms of hydrogen consumption.

	M_{FC} (g)	$(M_{FC} - M_{PI})/M_{FC} \times 100$ (%)
NEDC	3.267	20
UDDS	3.869	25
NYCC	1.214	27
Japan. 10–15	2.106	23
HWFET	3.636	12
US06	2.106	24

than the fuzzy controller, which gives the former the advantage in terms of hydrogen consumption. The power contribution of the fuel cell side of the hybrid power source is shown in Fig. 16. The rest power is met by the battery.

A more comprehensive comparison between the PI and fuzzy controllers is illustrated in Fig. 17 for US06. The fuel consumption of the two controllers, together with the off-line optimum, is evaluated as a function of the difference between the final and initial SOC. For the off-line optimum, the measurements are collected for different final SOC between 0.55 and 0.65 in open loop as described in Section 6.1. In closed loop, the initial SOC was varied between 0.55 and 0.65 for the PI controller, and between 0.5 and 0.6 for the fuzzy controller. Linear polynomial fits to the data are shown in Fig. 17 for an easy comparison. The fuel consumption of the PI controller is barely distinguishable from the off-line optimum. The intercept of the fit line represents the hydrogen consumption for the perfect charge sustenance (i.e., final SOC = initial SOC). The charge sustenance is achieved by the PI controller for an initial SOC of 0.608 and the corresponding hydrogen consumption is 1.616 g, which is exactly the same consumption of the off-line optimum. The fuzzy controller achieves the perfect charge sustenance for an initial SOC of 0.546 with a consumption of 1.639 g. So, the PI controller saves about 1.4% of hydrogen in comparison to the fuzzy controller when both controllers achieve the charge sustenance. More accurately, for a quadratic polynomial fit to the data, the calculated hydrogen saving becomes 1.7%, which is almost the same as the one reported in Table 3. Lastly, in comparison to the single-valued evaluation used in Table 3, the experimental evaluation illustrated in Fig. 17 gives a more comprehensive overview of the performance of the real-time controllers; however, it requires quite extensive experimental measurements.

The advantage of hybridization with respect to hydrogen consumption was evaluated by measuring the hydrogen consumption when only the fuel cell system is used to drive the load; however, the battery was kept connected to the bus to absorb the recuperated energy. The measured consumptions, M_{FC}, over the evaluation driving cycles are listed in Table 4. Table 4 also lists the percentage hydrogen saving when the hybrid power source is controlled by the optimized PI controller in comparison to the pure fuel cell drive, where the hydrogen consumption of the PI controller, M_{PI}, is the equivalent consumption taken from Table 3. Over most of the evaluation driving cycles, the hydrogen saving ranges between 20% and 27%. The hybridization is less beneficial for HWFET, with only 12% hydrogen saving, due to the short regenerative braking phases for this highway cycle. Lastly, the values given in Table 4 should be cautiously considered, because several factors, such as the change in fuel cell system size and vehicle mass, are not taken into account and they may affect the hydrogen saving of the hybrid vehicle as compared to the non-hybrid.

7. Conclusion

The optimization of the power management of a fuel cell hybrid vehicle was investigated through simulation and experimentation. The off-line optimization using Pontryagin's Minimum Principle was, first, recalled to calculate the best hydrogen consumption that can be achieved when the complete load profile is known in advance. The off-line optimum was then used as a benchmark when optimizing the real-time power management strategy, where both hydrogen consumption and charge sustenance were taken into account as two separate performance indices. It was shown that the real-time strategy can be optimized over a set of driving cycles and not only one, which increases the robustness of the designed controllers when they are applied to real driving conditions. Two real-time controllers were tested: a PMP-based PI controller with three parameters and a fuzzy logic controller with ten parameters. Both simulation and experiment showed that the PI controller can achieve a better performance in terms of hydrogen consumption, even though it has fewer parameters to be optimized.

The performance of the optimized real-time controller depends on two main factors: the form of the controller and the number of parameters engaged in the optimization. For more parameters, a better performance would be expected when the chosen parameters are independent. Increasing the number of membership functions of the fuzzy controller would lead to a better performance in terms of hydrogen consumption and robustness. However, firstly, achieving a significant improvement in comparison to the simple PI controller is doubtful and, secondly, increasing the number of optimization parameters would, necessarily, require longer computation time in order to guarantee the global optimum.

Acknowledgments

The doctoral fellowship of the corresponding author, Farouk Odeim, is granted by the Atomic Energy Commission of Syria (Syria).

References

[1] X. Wei, L. Guzzella, V. Utkin, G. Rizzoni, J. Dyn. Syst. Meas. Control 129 (2007) 13–19.
[2] Donald E. Kirk, Optimal Control Theory, fourteenth ed., Dover Publications Inc., New York, 2004.
[3] Nikolce Murgovski, Lars Johannesson, Jonas Sjöberg, Bo Egardt, Mechatronics 22 (2012) 106–120.
[4] Xiaosong Hu, Nikolce Murgovski, Lars Johannesson, Bo Egardt, Appl. Energy 111 (2013) 1001–1009.
[5] Namwook Kim, Sukwon Cha, Huei Peng, IEEE Trans. Control Syst. Technol. 19 (2011) 1279–1287.
[6] P. Rodatz, G. Paganelli, A. Sciarretta, L. Guzzella, Control Eng. Pract. 13 (2005) 41–53.
[7] G. Paganelli, S. Delprat, T.M. Guerra, J. Rimaux, J.J. Santin, in: IEEE 55th Vehicular Technology Conference (VTC Spring 2002), 4, 2002, pp. 2076–2081.
[8] Antonio Sciarretta, Michael Back, Lino Guzzella, IEEE Trans. Control Syst. Technol. 12 (2004) 352–363.
[9] Lorenzo Serrao, Simona Onori, Giorgio Rizzoni, in: American Control Conference, 2009, pp. 3964–3969.
[10] Soon-il Jeon, Sung-tae Jo, Yeong-il Park, Jang-moo Lee, J. Dyn. Syst. Meas. Control 124 (2002) 141–149.
[11] Ivan Arsie, Marco Graziosi, Cesare Pianese, Gianfranco Rizzo, Marco Sorrentino, in: Proc. 7th Int. Symp. Adv. Vehicle Control (AVEC), 2004, pp. 483–488.
[12] J. Bernard, S. Delprat, T.M. Guerra, F.N. Büchi, Control Eng. Pract. 18 (2010) 408–417.
[13] Chan-Chiao Lin, Huei Peng, J.W. Grizzle, in: Proc. Am. Control Conf., 5, 2004, pp. 4710–4715.
[14] Stefano Barsali, Carmine Miulli, Andrea Possenti, IEEE Trans. Energy Convers. 19 (2004) 187–195.
[15] Chan-Chiao Lin, Huei Peng, J.W. Grizzle, Jun-Mo Kang, IEEE Trans. Control Syst. Technol. 11 (2003) 839–849.
[16] S. Caux, W. Hankache, M. Fadel, D. Hissel, Int. J. Hydrogen Energy 35 (2010) 2134–2143.
[17] Chun-Yan Li, Guo-Ping Liu, J. Power Sources 192 (2009) 525–533.
[18] Xiaosong Hu, Shengbo Li, Huei Peng, J. Power Sources 198 (2012) 359–367.
[19] FreedomCAR Battery Test Manual for Power-assist Hybrid Electric Vehicles, Idaho National Engineering and Environmental Laboratory (INEEL), October 2003.
[20] Arthur E. Bryson Jr., Yu-Chi Ho, Applied Optimal Control, Revised Printing, Taylor & Francis Group, New York, 1975.
[21] Thijs van Keulen, Fuel Optimal Control of Hybrid Vehicles, PhD Thesis, Technische Universiteit Eindhoven, 2011, pp. 47–52.
[22] C.H. Zheng, C.E. Oh, Y.I. Park, S.W. Cha, Int. J. Hydrogen Energy 37 (2012) 1790–1796.
[23] A. Chasse, G. Corde, A.D. Mastro, F. Perez, in: IEEE Vehicle Power and Propulsion Conference (VPPC), 2010, pp. 1–6.
[24] J. Kessels, M. Koot, P. van den Bosch, D. Kok, IEEE Trans. Veh. Technol. 57 (2008) 3428–3440.
[25] Mitsuo Gen, Runwei Cheng, Genetic Algorithms and Engineering Optimization, John Wiley & Sons Inc., New York, 2000.